N-Arylhydroxamic Acids as Novel Oxidoreductase Substrates

Juozas Kulys,*[a] Heinz-Josef Deussen,[b] Kastis Krikstopaitis,[a] Rikke Lolck,[b] Palle Schneider,[b] and Arturas Ziemys[c]

Keywords: Oxidoreductases / Redox chemistry / Electrochemistry / Ab initio calculations / Structure−activity relationships

N-Arylhydroxamic acids (AHAs) are promising novel N–OH mediators for oxidoreductase catalysis. They are electrochemically active compounds with a redox potential of 0.31–0.41 V vs. SCE. Representative oxidoreductases, e.g. fungal peroxidase from *Coprinus cinereus* (rCiP), catalyze the oxidation of AHAs with apparent bimolecular constants (k_{ox}) of $7.1{\cdot}10^3$ to $1.5{\cdot}10^7$ $m^{-1}s^{-1}$ at pH = 8.5 and 25 °C. The limiting step in substrate oxidation was the reduction of compound II (Cpd II). The oxidation constants of *N*-hydroxyacetanilide (**1a**) and *N*-hydroxy-*N*-phenylbenzamide (**2a**), determined by a stopped-flow and steady-state method, were similar. The decrease in the reduction rate of Cpd II reduction rate decrease occurred at pK_a = 8.5 for **1a** and 7.7 for **2a**. The nitroxyl radical of **1a**, an intermediate in the oxidation, shows decreasing stability at alkaline pH. The structure–activity relationships (SARs) of these AHAs were analyzed within the framework of Marcus cross-relationship, and by using ab initio quantum chemical calculations. A linear correlation of log(k_{ox}) vs. redox potential was only indicated for benzamides, as predicted by electron transfer theory. Acetamides showed the opposite tendency: the constant (k_{ox}) increased if the potential of substrate increased. The correlation between log(k_{ox}) and HOMO (Highest Occupied Molecular Orbital) energy revealed that for benzamides the reactivity decreased with decreasing HOMO energy, whereas for acetamides the reactivity increased if the HOMO energy decreased. The rather low reactivity of these AHAs and the unexpected dependence on the redox potential and the HOMO energy could be explained by the electronic structure of the AHAs and the substrates docking in the active center of the enzyme.

Introduction

Mediator-assisted oxidoreductase-catalyzed systems have gained increasing attention for various applications. They are currently being used in e.g. analytical chemistry, and have been explored for application in dye, paper, and pulp bleaching for many years.[1−4] In all these systems the enzymes catalyze the oxidation of a redox-active small molecule, the mediator (MH). The oxidized mediator then chemically oxidizes the target molecule (non-substrate) and is consequently reduced. The mediator thereby switches between its oxidized and reduced state. In the case of peroxidase, the most often employed enzyme, the mediator-assisted scheme for the conversion of the target molecule can be drawn as shown in Equation (1) to Equation (4), where E is the heme peroxidase in the resting state, compound I (Cpd I) and compound II (Cpd II) are intermediates that have two and one oxidation equivalent in comparison to the resting state, MH is the peroxidase substrate, and M$^{\cdot}$ is its oxidized state. The second-order rate constants of the corresponding reactions [Equation (1) to Equation (3)] are k_1, k_2, and k_3.

$$E + H_2O_2 \xrightarrow[k_2]{k_1} \text{Cpd I} + H_2O \quad (1)$$

$$\text{Cpd I} + MH \xrightarrow[k_3]{} \text{Cpd II} + M^{\bullet} + H^+ \quad (2)$$

$$\text{Cpd II} + MH + H^+ \rightarrow E + M^{\cdot} + H_2O \quad (3)$$

$$M^{\cdot} + \text{Target molecule} + H^+ \rightarrow \text{Product} + MH \quad (4)$$

Among peroxidases, a fungal peroxidase from the ink cap mushroom *Coprinus cinereus* (CiP) is of particular interest due to its high activity, especially at alkaline pH, its broad substrate specificity, and its low production cost.[5,6] By using recombinant DNA techniques the *Coprinus cinereus* peroxidase gene has been expressed in *Aspergillus oryzae*, and the enzyme can be obtained in high yield on an industrial scale.[6]

Phenols and aromatic amines are typical substrates of peroxidases.[7,8] CiP-catalyzed oxidation of single-electron donors, i.e. *N*-substituted phenylenediamines, phenothiazines, and phenoxazines were explored and the rate approaching diffusion limit has been established for some of these substrates.[9−11] Aromatic N−OH derivatives, where the nitrogen atom is part of the heterocycles, were earlier suggested as promising mediators in peroxidase- and lactase-catalyzed dye and lignin bleaching, as well as lignin degradation.[3] Kinetics of enzymatic oxidation of *N*-hydroxybenzotriazole (HBT) was explored in ref.[12] The unexpected low reactivity of the HBT was attributed to the high redox potential of this substrate.

The derivatives of *N*-arylhydroxamic acid (AHA), i.e. compounds containing R−CO−N(OH)−Ar as a structural

[a] Institute of Biochemistry,
Moksliniku 12, 2600 Vilnius, Lithuania
E-mail: jkulys@bchi.lt
[b] Novozymes A/S,
Smørmosevej 9, 2880 Bagsværd, Denmark
[c] Vytautas Magnus University, Environmental Faculty, Department of Biology,
Vileikos 8, 3500 Kaunas, Lithuania

  1434−193X/01/0918−3475 $ 17.50+.50/0

subunit, represent a promising new type of N−OH mediator for oxidoreductase catalysis.[13] The structures of the AHA derivatives **1a**−**e**, **2a**−**d**, **3**, **4**, and **5** are shown in Scheme 1.

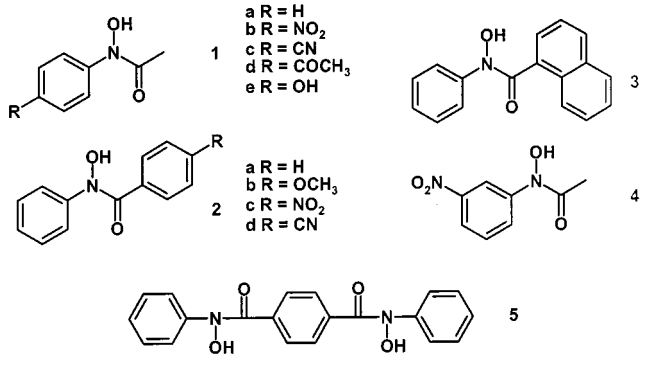

Scheme 1. Structure of *N*-arylhydroxamic acids

The aim of this work was to synthesize a series of *N*-arylhydroxamic acids and to explore the redox properties of AHAs and the kinetics of rCiP-catalyzed AHAs oxidation with an emphasis to structure−activity relation (SAR). To achieve this goal, the kinetics of the enzymatic reaction was investigated at steady-state and pre-steady-state conditions. SARs were elucidated by using ab initio quantum chemical calculations and substrate docking simulations.

Results and Discussion

N-Arylhydroxamic acids were synthesized as described in the Exp. Sect. The redox properties of AHAs were investigated by cyclic (CV) or differential-pulse voltammetry (DPV) at pH = 4.0−10.0. The CV of **1a** showed fine expressed oxidation and reduction peaks. The difference between anodic and cathodic peaks changes from 82 to 157 mV, demonstrating a quasi-reversible character of **1a** conversion (Table 1). The calculated formal oxidation-reduction potential of **1a** was 370 mV vs. SCE at pH = 8.5. It was dependent on the pH of the buffer solution (Table 1).

Table 1. The potential values (vs. SCE) of the oxidation-reduction of *N*-hydroxyacetanilide (**1a**) on a glassy carbon electrode; scan rate 100 mV/s, 0.1 M tri-component buffer solution containing 0.1 M KCl

Solution pH	$E_{p,a}$ [mV]	$E_{p,c}$ [mV]	E [mV]
4.0	623	473	548
4.5	571	449	510
5.0	554	405	480
5.5	551	394	472
6.0	503	389	446
6.5	475	337	406
7.0	430	338	384
7.5	423	344	383
8.0	422	326	374
8.5	411	329	370
9.0	413	321	367
9.5	420	312	366
10.0	415	312	363

At least two areas where the potential is dependent on the pH could be identified. One transition corresponded to a pK_a of 3.7±0.6 and the other to a pK_a of 6.3±0.1. At pH > 7.5 the potential changed little, therefore the electrochemical conversion could be explained as a single-electron transfer followed by a fast proton release:

$$CH_3-CO-N(OH)-Ph \rightarrow CH_3-CO-N^{+\cdot}(OH)-Ph + e^- \quad (5)$$

$$CH_3-CO-N^{+\cdot}(OH)-Ph \rightarrow CH_3-CO-NO^{\cdot}-Ph + H^+ \quad (6)$$

In the range pH = 3.7−6.3, the oxidation rate was limited by electron/proton transfer. At acidic pH (pH < 3.7) the nitrogen atom is most likely to be protonated and the redox conversion of this form proceeded at higher potential.

The cyclic voltammetric curves of the other AHA derivatives showed fine expressed anodic, but weak cathodic peaks, that have been associated with an irreversible electrochemical conversion. Therefore, a formal redox potential of these substrates was determined using DPV. The values of the calculated potentials of AHAs at the pulse height 25, 50, and 100 mV varied, with exception of **2a**, within a 5-mV range. The calculated value for **2a** showed a tendency of increasing potential by 8 mV, if the pulse height increased from 25 to 50 and 100 mV. This indicated a completely irreversible character for the conversion. The formal potential of this compound was averaged from the potential values at 25, 50, and 100 mV pulse heights. The values of the formal redox potentials of all AHAs covered a range from 306 to 411 mV (Table 2).

In order to compare the redox activity of AHAs with those of unsubstituted hydroxamic acids, the CV of benzhydroxamic acid (BHA) was recorded at pH = 8.5. In contrast to AHAs, BHA produced a broad oxidation peak and showed completely irreversible character for the electrochemical oxidation. An approximate value of 0.4 V of the formal redox potential of BHA determined from half-wave potential was used for the following comparisons.

The AHAs showed the maximum absorbance in the range of 240−320 nm. During rCiP-catalyzed oxidation the absorbance spectra of the substrates changed. In the case of **1a** the product showed two absorbance peaks at 282 and 306 nm. An isosbestic point during **1a** oxidation was observed at 266 nm. The spectrum of the formed product very closely resembled the spectrum of nitrosobenzene (NB) (Figure 1). During enzymatic oxidation of **1a** at pH = 5.5 a new band with absorbance at 318 nm appeared at the beginning of the reaction (Figure 2). This band has been attributed to the absorbance of the intermediate product.

The formation of NB during enzymatic oxidation of **1a** was additionally confirmed by gas chromatography. Upon incubation of a 10 mM solution of **1a** in the presence of 200 nM of rCiP and 7 mM of hydrogen peroxide, 6.9 mM of NB was formed during 7 h at pH = 8.5.

The formation of NB during the oxidation of **1a** can be explained by a single-electron oxidation of the substrate with Cpd I and Cpd II, followed by a disproportionation of the formed radical, and the reaction of the resulting two

Table 2. Absorbance, electrochemical, and kinetic parameters of *N*-arylhydroxamic acids at pH = 8.5 and 25 °C

Compound	*E* [mV] vs. SCE)	λ_{max} [nm]	$\Delta\varepsilon$ [$mM^{-1}cm^{-1}$]	k_{ox} [$M^{-1}s^{-1}$]
1a	370±2	310	8.9	$(7.1\pm0.2)\cdot10^3$
2a	375±6	310	10.7	$(9.9\pm0.3)\cdot10^4$
1b	411±2	288	5.4	$(2.5\pm0.1)\cdot10^5$
2b	313±2	280	5.8	$(1.5\pm0.1)\cdot10^5$
1c	406±1	285	3.1	$(8.5\pm0.6)\cdot10^3$
2c	375±4	281	3.1	$(7.1\pm0.4)\cdot10^4$
1d	393±2	288	3.1	$(9.2\pm2.1)\cdot10^4$
2d	391±3	307	4.3	$(5.0\pm0.3)\cdot10^4$
1e	369±1	244	5.1	$(1.5\pm0.2)\cdot10^7$
3	364±2	310	6.5	$(8.3\pm0.6)\cdot10^3$
4	403±1	256	2.0	$(9.2\pm0.6)\cdot10^3$
5	307±2	279	4.7	$(8.7\pm0.4)\cdot10^5$

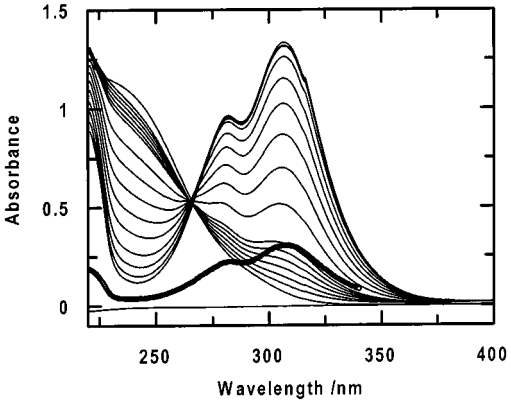

Figure 1. Absorbance changes of *N*-hydroxyacetanilide (**1a**) (solid curves) during enzymatic oxidation in 50 mM borate buffer solution at pH = 8.5 and absorbance of nitrosobenzene (NB) (circles) in the same buffer solution; concentration of the substrate 0.2 mM, rCiP 208 nM, H_2O_2 0.5 mM, NB 50 μM; incubation time: 0 (blank), 0, 0.5, 3, 6, 9, 12, 15, 30, 45, 60, 75, 90, 105, 120, 135, and 150 min

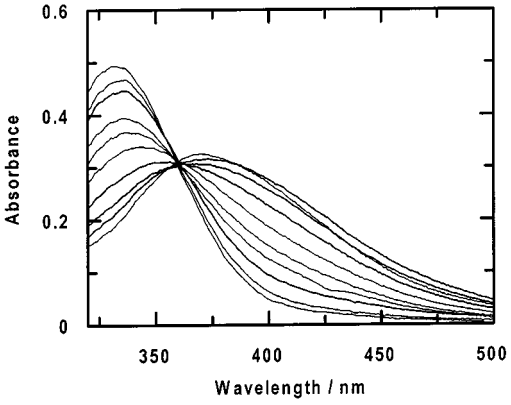

Figure 2. Absorbance changes of *N*-hydroxyacetanilide (**1a**) during enzymatic oxidation in 50 mM acetate buffer solution at pH = 5.5; concentration of the substrate 0.2 mM, rCiP 208 nM, H_2O_2 0.5 mM; incubation time: 0, 0.5, 3, 6, 9, 15, 18, 21, 24, 27, 30, 33, 36, 39, 42, 45, 48, 51, 54, 57, and 60 min

electron oxidized species with water [Equation (7) to Equation (9)].

$$2\,CH_3{-}CO{-}N(OH){-}Ph \rightarrow 2\,CH_3{-}CO{-}NO^{\cdot}{-}Ph + 2\,H^+ + 2\,e^- \quad (7)$$

$$2\,CH_3{-}CO{-}NO^{\cdot}{-}Ph + H^+ \rightarrow CH_3{-}CO{-}N(OH){-}Ph + [CH_3{-}CO{-}NO^+{-}Ph] \quad (8)$$

$$[CH_3{-}CO{-}NO^+{-}Ph] + H_2O \rightarrow PhNO + CH_3COO^- + 2\,H^+ \quad (9)$$

The formation of the **1a** radical during the enzymatic reaction according to Equation (7) could furthermore be confirmed by ESR measurements. A triplet of multiplets was observed (Figure 3), which is typical for a radical with a free electron localized in the proximity of a nitrogen atom.[14]

The investigation of the kinetics of the generation of the **1a** radical revealed that the radical was most stable at pH = 5.5 (Figure 4). At pH = 8.5 the stability of the radical was very low. The investigation of the decomposition of the AHA **1a** radical at pH = 5.5, generated by using 5, 10, and 15 μM of H_2O_2, gave the second-order reaction constant 150±6 $M^{-1}s^{-1}$.

The ESR measurements confirmed the postulated mechanism of the **1a** radical formation and decomposition. The characteristics of the absorbance spectra at pH = 5.5 (Figure 2) together with the observed decomposition of the radical (Figure 4) allowed to conclude that the absorbance at 318 nm belonged to the **1a** radical. The distinct absorption of that radical did not appear at pH = 8.5 due to low stability of the radical. Preliminary investigations also showed that the conversion of **2a** proceeded in a similar manner as with **1a**.

For the calculations of the kinetic parameters of **1a** oxidation, a wavelength of 310 nm was chosen (Table 2). At that wavelength the largest absorbance change was observed. During oxidation of **1b** the largest absorbance change was indicated at 288 nm. The maximum absorbance of the product formed during the oxidation of **1c** was detected at 285 nm. The largest change of the absorbance for **5**, **2b**, **1d**, and **2e** was at 279 nm, 280 nm, 288 nm, and 244 nm, respectively (Table 2). The kinetics of the **2c** oxida-

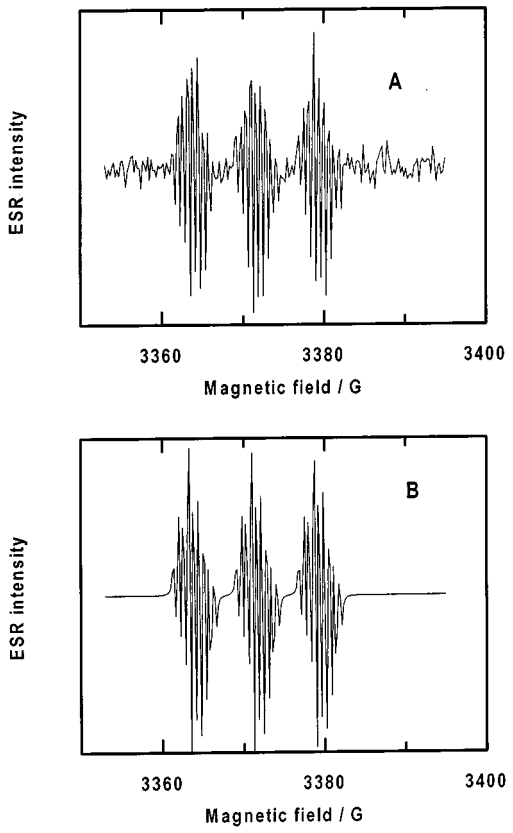

Figure 3. The ESR spectrum of the radical of *N*-hydroxyacetanilide (**1a**) formed upon enzymatic oxidation at pH = 7.0 (A); the "B" shows the simulated spectra with the hyperfine splitting: three H atoms (aromatic *ortho* and *para*): 1.2 G, two H atoms (aromatic *meta*): 0.68 G and one N atom: 7.7 G; line width 0.2 G, g = 2.006850

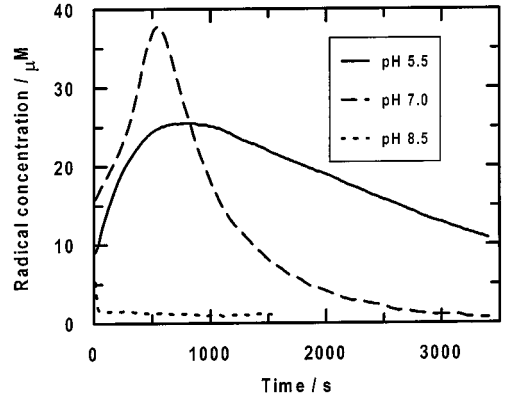

Figure 4. The kinetics of *N*-hydroxyacetanilide (**1a**) radical formation at different pH values observed by ESR

tion was measured at 281 nm. The largest change of absorbance during the oxidation of **3** was observed at 310 nm. The maximum absorbance change for the oxidation of **5** was at 256 nm. Upon oxidation of **2d** new absorbance peaks appeared at 282 and 307 nm. The calculated extinction coefficient of oxidized **2d** at 307 nm as well as the results of the absorbance changes of other investigated substrates are listed in Table 2.

The initial rate of rCiP-catalyzed **1a**, **2a**, **3**, **5**, **2d**, **1b**, **5**, **2d**, **2b**, and **2c** oxidation increased linearly with increasing substrate concentration. The dependencies of the initial oxidation rates of **1d** and **1e** on the substrate concentrations were found to be hyperbolic. K_m was calculated to be 112 μM for **1d** and 59 μM for **1e**. The calculated k_{ox} are listed in Table 2. The calculated value of k_{ox} for **1d** was similar to those of the other compounds, whereas the constant for **1e** was 163 times larger (Table 2).

The rapid-scan spectra of the mixture of ferri peroxidase and hydrogen peroxide at pH = 8.5 showed a fast formation of compound I and its auto reduction to compound II. Due to auto reduction of the compound I at this pH, the reaction with **1a** started by mixing an enzyme/**1a** solution with hydrogen peroxide. At these conditions the reduction of Cpd II was slow (Figure 5). The kinetics of Cpd II decay as well as of ferri rCiP formation fitted the first-order reaction scheme at 4−50 times excess of **1a** (Figure 5).

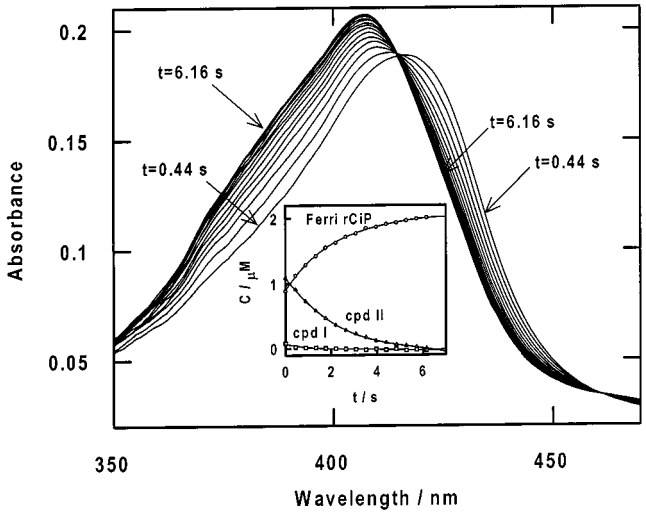

Figure 5. The changes in the concentration of the intermediates of rCiP during the reaction with *N*-hydroxyacetanilide (**1a**) at pH = 8.5; rCiP 2 μM, H_2O_2 2 μM, **1a** 50 μM, interval between the spectra 440 ms

The first-order reaction constant (k) of the Cpd II reduction was dependent on the AHA **1a** concentration. An apparent k_3 calculated as k/[**1a**] was $(9.5\pm0.7)\cdot10^3$ $M^{-1}s^{-1}$ at pH = 8.5 and 50 μM of the substrate. This increased to $(12.2\pm0.2)\cdot10^3$ $M^{-1}s^{-1}$ at a **1a** concentration of 0.1 mM. The k_3 value at 50 μM was similar to the value $(7.1\pm0.2)\cdot10^3$ $M^{-1}s^{-1}$ determined at steady-state conditions. The reduction of Cpd II with **1a** revealed a reaction constant maximum at pH = 7 (Figure 6) and a decrease of the constant at alkaline pH, with an apparent pK_a of 8.5±0.2 in the pH range from 6 to 9.

The rapid-scan experiments showed that at pH = 6−9 the limiting step of oxidized peroxidase reduction with **2a** was also Cpd II reduction. However, at pH = 8.5 the bimolecular constant was 15 times larger in comparison with the constant of **1a**. A similar ratio of the constants was determined from steady-state measurements (Table 2). The max-

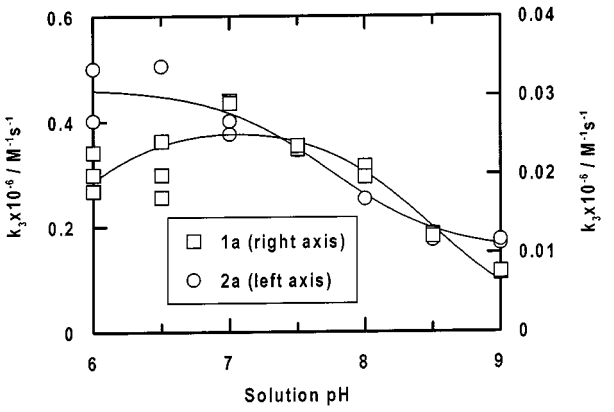

Figure 6. The dependence of the kinetic constants of Cpd II reduction with **1a** and **2a** on the pH at 25 °C; concentration of rCiP 2 μM, H_2O_2 2 μM, **1a** and **2a** 0.1 mM, 20 mM tri-component buffer solutions

imum value of the constant was found at pH = 6.5, and the apparent pK_a of activity decrease was at 7.7±0.2.

The reaction of the benzhydroxamic acid (BHA) with oxidized peroxidase was also limited by Cpd II reduction. At pH = 7.0 the apparent bimolecular constant was $(1.6\pm0.2)\cdot10^6$ $M^{-1}s^{-1}$. This value was similar to the constant $1.1\cdot10^6$ $M^{-1}s^{-1}$ at pH = 7.4 determined in the reaction of ARP with BHA under steady-state conditions.[15] The constant decreased up to $(0.11\pm0.03)\cdot10^6$ $M^{-1}s^{-1}$ at pH = 8.5.

Ab initio calculations of AHAs showed that the molecular structures of all molecules are non-planar (Figure 7). In **1a** the *N*-aryl and the carbonyl groups are twisted by 15−20°. The hydroxylamine residue and the *N*-aryl group lie almost in the same plane: The dihedral angle is about 8−10° for benzamides and about 1° for acetamides. This indicates a strong conjugation of the nitrogen atom and the *N*-aryl fragment. During the oxidation of the AHAs, the structure of the formed radicals became completely flat showing a strong electronic conjugation between *N*-aryl, hydroxylamine, and the carbonyl groups (Table 3). Calculations of MOs (sum of MO coefficients of the atoms) of AHAs show that the main contribution to the HOMO comes from N; C3 and C6 confirm a strong electronic conjugation of *N*-aryl and N−OH groups (Figure 8). The calculations of bond orders showed that the main rearrangements in geometry and electronic structure during oxidation take place in the vicinity of the N−OH fragment (Figure 9).

The calculated HOMO energies of AHAs in the ground state changed in the range between −0.3535 a.u. and −0.2972 a.u. (1 a.u. = 27.2116 eV) when the RHF/6-31G method was used. Since **1e** is a phenol derivative, where the phenolic −OH group can also be oxidized, it was analyzed separately. The other AHAs can be divided into two groups of similar electrochemical behaviour: acetamides (**1a**-like compounds) and benzamides (**2a**-like compounds). The calculated HOMOs of the substrates are listed in Table 4. The averaged HOMO of benzamides was about 0.015−0.02 a.u. higher in comparison to those of the acetamides.

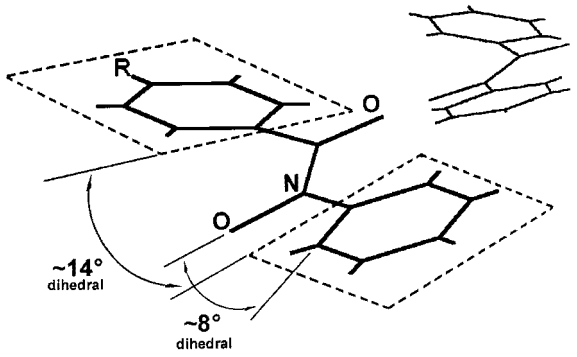

Figure 7. Calculated molecular structure of *N*-hydroxy-*N*-phenylbenzamide (**2a**)

Table 3. Calculated parameters for compounds **1a** and **2a**

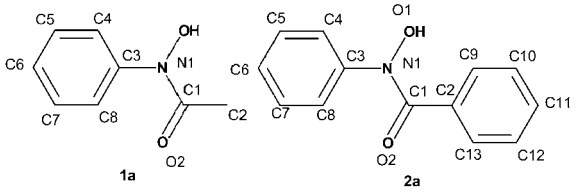

Parameter	2a			1a		
	AHA	AHA˙	Δ	AHA	AHA˙	Δ
Bond lengths [Å]						
N1−O1	1.426	1.354	−0.072	1.430	1.361	−0.069
N1−C1	1.376	1.400	0.024	1.380	1.400	0.020
N1−C3	1.425	1.440	0.015	1.420	1.430	0.010
C1−O2	1.220	1.216	−0.004	1.215	1.210	−0.005
C1−C2	1.499	1.505	0.006	1.510	1.509	−0.001
C3−C4	1.390	1.390	0.000	1.388	1.389	0.001
C4−C5	1.380	1.379	−0.001	1.381	1.380	−0.001
C5−C6	1.383	1.383	0.000	1.382	1.384	0.002
C6−C7	1.382	1.380	−0.002	1.383	1.381	−0.002
C7−C8	1.382	1.385	0.003	1.382	1.384	0.002
C2−C9	1.389	1.391	0.002			
C9−C10	1.384	1.383	−0.001			
C10−C11	1.383	1.381	−0.002			
C11−C12	1.384	1.384	0.000			
C12−C13	1.379	1.378	−0.001			
Angles [°]						
C3−N1−C1	128.7	127.4	−1.3	128.9	128.0	−0.9
N1−C1−C2	120.3	122.0	1.7	115.0	114.5	−0.5
Torsion angles [°]						
C4−C3−N1−O1	−8.2	0.0	8.2	3.1	0	−3.1
C8−C3−N1−C1	−14.3	0.0	14.3	19.4	0	−19.4
C9−C2−C1−O2	28.7	0.0	−28.7			
C13−C2−C1−N1	21.3	0.0	−21.3			
C3−N1−C1−C2	−169.5	−180.0	−10.5	19.7	180	160.3

HOMO and geometry calculations showed a significant conjugation between the π-electrons of the *N*-aryl and the N−OH group. Titration of **1b** (containing a nitro group at the C6 position) confirmed the conclusion; **1b** showed an absorbance change at pH = 7.05−11.83 with a pK_a of the transition of 8.37±0.04 (Figure 10).

The absorbance change was associated with heterolytic NO−H bond dissociation. The dissociated form absorbed at longer wavelength (Figure 10). In contrast, if the nitro group was at the C11 position of the benzamide residue,

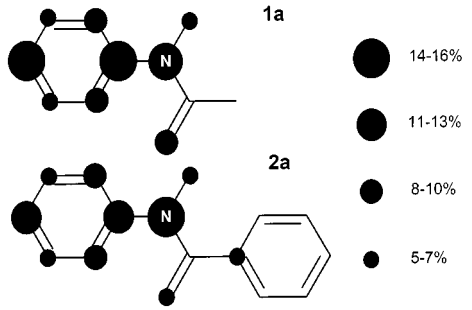

Figure 8. MO coefficients for the HOMO of **1a** and **2a**; atoms with less than 5% donation to the HOMO are not shown

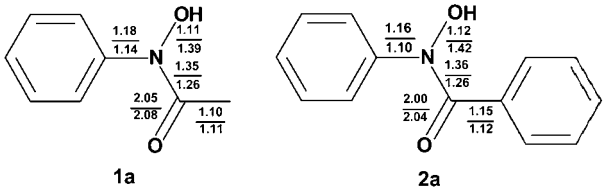

Figure 9. Bond orders of reduced substrates (upper numbers) and their oxidized states (lower numbers) of **1a** and **2a**

Table 4. Calculated HOMO energies of AHAs

Compound	RHF/6-31G [a.u.]
1a	−0.3140
1b	−0.3535
1c	−0.3339
1d	−0.3259
1e	−0.3025
2a	−0.3125
2b	−0.3094
2c	−0.3278
2d	−0.3236
3	−0.2972
4	−0.3475
5	−0.3162

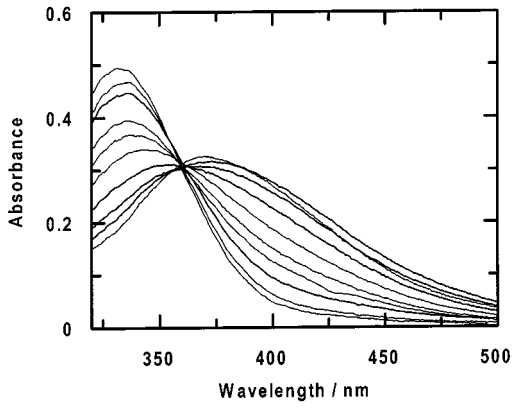

Figure 10. Absorbance of *N*-hydroxy-*N*-(4-nitrophenyl)acetamide (**1b**) at different pH values (pH = 7.05, 7.38, 7.71, 8.08, 8.32, 8.60, 9.00, 9.42, 9.84, and 11.83); the absorbance increases with increasing pH at wavelengths larger than 360 nm

like in **2c**, the absorbance changed significantly less in the same interval of pH.

Quantum chemical calculations were used to evaluate SAR of AHAs. According to the electrochemical investigations, AHAs are electrochemically active compounds. The oxidation of AHAs was associated with an electron transfer from the HOMO. Therefore, the values of redox potential (E) were correlated with the HOMO energies. The correlation coefficient (R^2) of the linear dependence of E and the HOMO energies, with exception of **1e**, was 0.44. If **2b** and **5** were omitted from the correlation the R^2 were all 0.83. The peculiarities of **2b** and **5** might be explained by the structure of the HOMO. The calculations showed that the HOMO of **2b** expanded more over the whole molecule in comparison to other benzamides. The HOMO of compound **5**, in contrast to the other compounds, shows a symmetrical shape for the MO, therefore the probability of electron transfer increases.

The rate of rCiP-catalyzed oxidation of **1e** was higher than for all other acetamides and benzamides (Table 2). The high oxidation rate of AHA **1e** could be explained by oxidation of the phenolic −OH group, and was therefore omitted from further considerations. The reactions of the remaining AHAs were found to be limited by Cpd II reduction. If electron transfer is predominantly chemically controlled, the reactivity of Cpd II towards the AHAs should be related to the free energy of the reaction (to the thermodynamic driving force) as it is the case for other electron donors.[9,11,16] However, only a tendency of linear correlation of the log(k_{ox}) with the respective redox potentials could be observed for benzamides, as predicted by electron transfer theory[17] (Figure 11). For acetamides an opposite tendency was found: The constant (k_{ox}) increased with increasing substrate potential. The correlation coefficient was $R^2 = 0.42$. This revealed that the reactivity decreases if the HOMO energy decreased. For acetamides, on the other hand, the reactivity increased if the HOMO energy decreased, although the correlation was poor, i.e. $R^2 = 0.19$.

The rather low reactivity of AHAs and the unexpected correlations of log(k_{ox}) and HOMO energies could be explained by the electronic structure of AHAs and the substrates docking in the active center of CiP. As the crystal

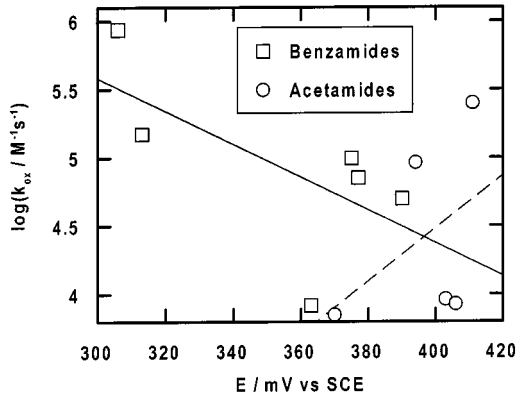

Figure 11. Correlation of the reactivity of AHAs with their redox potential at pH = 8.5

structure of fungal peroxidase *Arthromyces ramosus* (ARP) and recombinant CiP are almost the same − the primary structure of these peroxidases is different by one terminal amino acid[15,18] − the docking of AHAs in the active center of rCiP was analyzed in analogy to BHA docking in the active center of ARP.

The results of the substrates docking calculations revealed that the docking of BHA fits the crystallographic data, if the ARP structure is taken from the ARP/BHA complex (HSR in further discussion).[19] The docking calculations of **1a** in the HSR structure revealed two possible ways for the substrate complexation to take place (Figure 12). The mean docking energies were −6.43 kcal/mol and −6.40 kcal/mol for the first and the second cluster, respectively. The small difference between energies indicates that about 73% of **1a** occupy the first cluster and 27% the second cluster. In both clusters the benzene ring is located at the entrance of the heme cavity and N−OH and CO groups were placed inside the active center. In the first cluster the methyl group and oxygen atom are connected to a water molecule that lies at the distal side of heme between the histidine residue and the iron atom. The structure of this cluster is almost identical to the ARP/BHA cluster. In the second cluster, **1a** is rotated 180° around the *N*-phenyl axis and is a little bit twisted while the water molecule interacts with the C=O group (Figure 12).

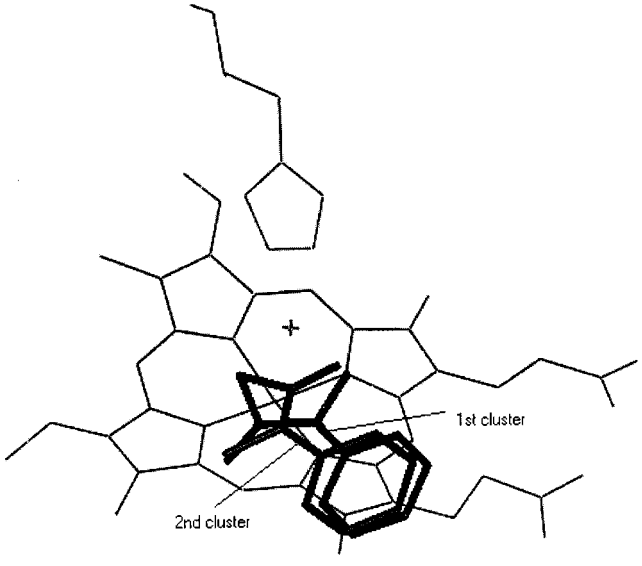

Figure 12. Docking of **1a** in the active center of HSR; the asterisk shows a water molecule

The calculations of **2a** docking in the HSR structure revealed two complexation sites in the vicinity of the heme. The largest amount (96.6%) of **2a** was docked in a small pocket formed by Ile 153 and Pro 91 (Figure 13). The mean docking energy of about 80% of these complexes was −7.33 kcal/mol. In the second type of clusters **2a** is located at the entrance to the heme. It has a mean docking energy of −6.11 kcal/mol and occupies 4.4% of all structures. In this cluster **2a** lies almost parallel to the heme plain and is placed very close to methyl and propionic acid residues of the heme.

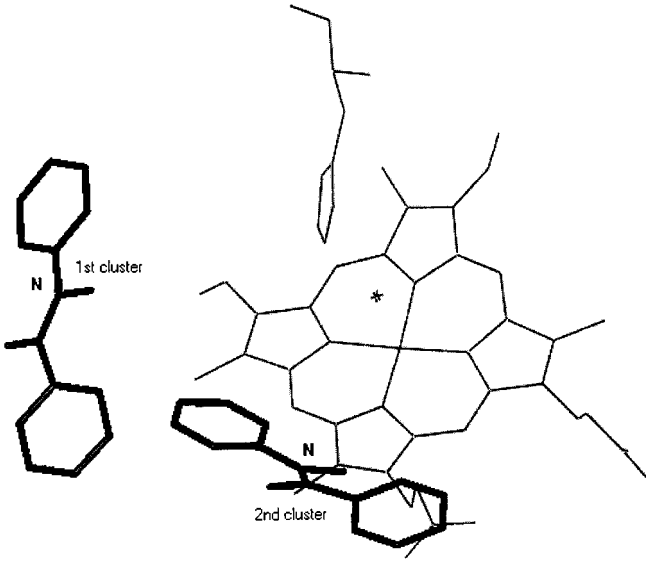

Figure 13. Docking of **2a** in the active center of ARP; the asterisk shows a water molecule

The docking results thus reveal differences in complexation of the acetamides **1a**−**1d**, **4** and the benzamides **2a**−**2d** and **3** in the active center of peroxidases. According to quantum chemical calculations, the main fraction of the HOMO of AHAs is located on the *N*-aryl substituent. The same residue in the second cluster of **2a** combines more closely with the heme in comparison to **1a**. Moreover, the carbon atom of **2a** in the *para* position of the *N*-aryl-substituted benzamide is about 1.2 Å closer to a water molecule and about 0.6 Å closer to the heme plane than in **1a**. This location permits more effective orbital overlapping, and can explain why benzamides show greater reactivity than the acetamides. Therefore, for benzamides there possibly exists a good correlation ($R^2 = 0.95$) of reactivity with the sum of atom charges in the *ortho* (C9, C13) and *meta* positions (C10, C12) of the benzamide ring, and their reactivity obeys electron transfer theory.[17] In contrast to benzamides, the complexation of acetamides retards effective *N*-phenyl and heme orbital overlapping. Therefore, the reactivity of the substrates decrease. These considerations permit us to speculate that the main factor controlling the electron transfer rate becomes substrate docking rather than the free energy of the reaction. Possibly for this reason, the reactivity of BHA is comparable with acetamides since the docking areas and redox potentials are similar.

In summary, *N*-arylhydroxamic acids are electrochemically active redox compounds showing interesting features as new mediators for peroxidase catalysis, as was previously demonstrated for lactase-catalyzed processes.[13] The intermediate in the oxidation of **1a** is a nitroxyl radical, and the final oxidation product has been identified as nitrosoben-

zene. Quantum chemical calculations revealed specific electronic structure. Docking calculations of the AHAs gave a better understanding of the structure−activity relationship of these substrates.

Experimental Section

N-Hydroxyacetanilide (**1a**),[20] *N*-hydroxy-*N*-(4-nitrophenyl)-acetamide (**1b**),[21] *N*-(4-cyanophenyl)-*N*-hydroxyacetamide (**1c**),[22] *N*-(4-acetylphenyl)-*N*-hydroxyacetamide (**1d**),[23] *N*-hydroxy-*N*-(4-hydroxyphenyl)acetamide (**1e**),[23,24] *N*-hydroxy-*N*-phenyl-4-methoxybenzamide (**2b**),[25,26] *N*-hydroxy-*N*-phenyl-4-nitrobenzamide (**2c**),[25,27] *N*-hydroxy-*N*-phenyl-1-naphthamide (**3**),[28,29] and *N,N′*-dihydroxy-*N,N′*-diphenylterephthalamide (**5**),[30] were prepared by acylation of the corresponding *N*-arylhydroxylamines with the corresponding acid chlorides according to the procedure described for AHA **1a** in ref.[20] All crystalline compounds were identified by ^{1}H NMR, ^{13}C NMR, and by the melting points given in the literature. − Benzhydroxamic acid (BHA), nitrosobenzene (NB), and *N*-hydroxy-*N*-phenylbenzamide (**2a**), were from commercial sources (Aldrich, Fluka). − ^{1}H NMR and ^{13}C spectra were recorded with a Bruker DRX 400 spectrometer with tetramethylsilane (TMS) as internal standard. − Elemental analyses were determined by PD Analytical Laboratories (Novo Nordisk A/S, MÅløv). − Melting points were determined with a Büchi 510 apparatus and are uncorrected. − Merck silica gel 60, 70−230 mesh ASTM was employed for column chromatography. Thin-layer chromatography was performed using Alugram SIL G/UV$_{254}$ TLC-plates from Macherey−Nagel. Gas chromatography was accomplished using an HP58 gas chromatograph 90 equipped with a capillary column and an FID detector.

4-Cyano-*N*-hydroxy-*N*-phenylbenzamide (2d): This compound was prepared from *N*-phenylhydroxylamine. A solution of *N*-phenylhydroxylamine (1.77 g, 16.2 mmol) in THF (30 mL) was synthesized according to ref.[20] A slurry of sodium bicarbonate (2 g in 2 mL of water) was added to the solution. The mixture was cooled to −2 °C and 4-cyanobenzoyl chloride (3.23 g, 19.51 mmol) was added dropwise. Stirring was continued overnight, before water (200 mL) was added. The reaction mixture was extracted (3 × 10 mL) with dichloromethane. The solvent from the combined organic phases was removed under vacuum. The residue was purified by chromatography using a Biotage Flash40i with SIM, fitted with a 4.0 × 15.0 cm cartridge, using AcOEt/heptane (3:5, v:v) as eluent, to give 0.55 g of pure **2d** (14%): m.p. 146−147 °C. − ^{1}H NMR (400 MHz, DMSO): δ = 10.93 (s, 1 H), 7.93 (d, 2 H), 7.80 (d, 2 H), 7.62 (d, 2 H), 7.42 (dd, 2 H), 7.24 (t, 1 H). − ^{13}C NMR (100 MHz, DMSO): δ = 165.91, 140.82, 139.59, 131.45, 128.38, 128.11, 125.43, 121.30, 117.85, 111.99. − $C_{14}H_{10}N_2O_2$ (238.2): calcd. C 70.58, H 4.23, N 11.76; found: calcd. C 70.62, H 4.32, N 11.64.

***N*-Hydroxy-*N*-(3-nitrophenyl)acetamide (4):** Hydrazine hydrate (3.56 g, 71.11 mmol) was added dropwise to a suspension of 1,3-dinitrobenzene (6.0 g, 35.69 mmol) and wet 5% rhodium/carbon (120 mg) in tetrahydrofuran (30 mL) while keeping the temperature below 15 °C. After stirring at room temperature overnight, the mixture was filtered and the catalyst washed with a little tetrahydrofuran. A slurry of sodium bicarbonate (6 g in 5 mL water) was added to the solution. The mixture was cooled to 0 °C and acetyl chloride (6.17 g, 78.60 mmol) was added dropwise. Stirring was continued overnight, followed by the addition of a solution of sodium hydroxide (5 g in 100 mL). The aqueous phase was separated, petroleum ether was added, and the tetrahydrofuran/petroleum ether phase was again separated. The combined organic phases were extracted with aqueous 10% sodium hydroxide solution. The combined aqueous phases were washed with CH_2Cl_2 and then neutralized with hydrochloric acid. The mixture was extracted with CH_2Cl_2 and the extracts were combined, dried with magnesium sulfate, filtered, and concentrated at reduced pressure. Upon the addition of petroleum ether, light orange crystals formed to give 4.59 g of pure **4** (66%): m.p. 92−94 °C. − ^{1}H NMR (400 MHz, $CDCl_3$): δ = 9.41 (1 H), 8.36 (1 H), 7.96 (1 H), 7.91 (1 H), 7.46 (1 H), 2.28 (3 H). − ^{13}C NMR (100 MHz, $CDCl_3$): δ = 149.01, 130.52, 127.42, 121.25, 116.43, 23.45. − $C_8H_8N_2O_4$ (196.2): calcd. C 48.98, H 4.11, N 14.28; found: calcd. C 49.55, H 4.16, N 14.21.

Recombinant Fungal Peroxidase from *Coprinus cinereus* (rCiP) is a product of Novo Nordisk A/S, Denmark. The enzyme was additionally purified by anion exchange chromatography to a Reinheit Zahl (A_{405}/A_{280}) of 2.61. The concentration of rCiP was determined spectrophotometrically at 405 nm by using the molar absorbance of $1.08\cdot10^5$ $M^{-1}cm^{-1}$.[5] Solutions of H_2O_2 were prepared from perhydrol (30%) and concentrations were established by using the molar absorbance of 39.4 $M^{-1}cm^{-1}$ at 240 nm.[31]

Steady-State Kinetics of substrate oxidation was performed by a spectrophotometric method. Kinetic curves and absorption spectra were registered by using a computer-assisted spectrophotometer (Gilford Instrument model 2600, Gilford Instrument Lab., USA). The measurements were carried out at 25±0.1 °C in 0.05 M borate buffer at pH = 8.5. The kinetic data for the change of absorbance were approximated to a third-order polynomial function. A relative error of approximation did not exceed 0.2%. The calculated initial steady-state rate was used for the further analysis. If the initial rate was a linear function of the substrate concentration, an apparent bimolecular rate constant (k_{ox}) was calculated from the slope of this dependence. If the rate showed saturating character, an apparent Michaelis constant (K_m) and catalytic constant (k_{cat}) was calculated according to the Michaelis−Menten equation. In this case, an apparent bimolecular rate constant (k_{ox}) was stated as the ratio of k_{cat}/K_m. All data are presented as mean ± standard deviation.

Pre-Stationary Kinetics of the substrate oxidation was performed using an Otsuka RA-401 stopped-flow spectrophotometer (Japan) interfaced with a computer system. Measurements were conducted by rapid scanning of the spectra. The gate time was 2, 4, and 440 ms; slit width was 1.4 nm; and wavelength ranged from 350 to 650 nm. The temperature was maintained at 25 °C by means of a circulating water bath. One syringe of the spectrophotometer contained 2 μM of CiP and 2 μM of H_2O_2, the other 2−20 μM of the substrate. In pre-stationary kinetics the quasi-first-order rate constant of ferri peroxidase formation and Cpd I/Cpd II reduction was calculated by fitting kinetic curves of absorbance changes at 394, 414, and 426 nm. These wavelengths correspond to an isosbestic point between Cpd I and Cpd II, to an isosbestic point between Cpd II and ferri peroxidase, and to an isosbestic point between Cpd I and ferri peroxidase, respectively.[5] The expressions of the kinetic curves of Cpd I, Cpd II, and ferri peroxidase concentration changes were derived in ref.[9] The buffer solutions for absorbance measurements were prepared from doubly distilled water. A 0.1 M buffer solution was prepared from 33 mM of sodium acetate, 33 mM of sodium dihydrophosphate and 33 mM of boric acid. A 20 mM tri-component buffer solution was prepared by 5 times dilution of the 0.1 M stock buffer solution.

The Cyclic Voltammograms were recorded in a three-electrode circuit by using a computer-controlled electroanalytical system (Cypress Systems, Inc., USA) and a glassy carbon electrode (model

Cs-1087, Cypress Systems, Inc., USA). As a reference, a saturated calomel electrode (SCE, saturated with KCl, mod. K-401, Radiometer, Denmark), and as auxiliary electrode a Pt wire (diameter 0.2 mm, length 4 cm), mounted on the end of the reference electrode, were used. The electrode potential was varied from 200 to 800 mV. The potential scan rate was 100 mV/s. The formal redox potential (E) was estimated by using the relationship $E = (E_{p,a} + E_{p,c})/2$, where $E_{p,a}$ and $E_{p,c}$ are the anodic and the cathodic peak potentials, respectively. The differential-pulse voltammetry (DPV) was performed by using the same electroanalytical system and electrodes. The formal redox potential was calculated as $E = (E_p + E_h/2)$, where E_p is a peak potential and E_h is a height of the pulse.

The Electron Spin Resonance (ESR) investigations of the radicals were performed with a Bruker EMX 113 ESR spectrometer with a ST4102 cavity. A borosilicate capillary tube was filled with 95 μL of the reaction mixture and placed in the cavity. Care was taken that the sample was placed at the same position each time. The measurements were performed at 22.5 °C. The ESR spectrum of the radical of **1a** was recorded after 4.7 min incubation of a 0.1 mM solution of **1a**, with 25 μM H_2O_2 and 16.7 nM rCiP in 10 mM phosphate buffer at pH = 7.0. The parameters were: sweep time 20.9 s, sweep width 41.720 G, center field 3373.66G, modulation amplitude 0.1 G, modulation frequency 100 kHz, frequency 9.469545 GHz, and power 2.007 mW. Simulation of the ESR spectrum was performed using the WINEPR SimFonia program by Bruker. The time profile of the radical was observed by monitoring the amplitude of the ESR signal after preparing the reaction mixture and introducing it into the instrument. The typical delay time from mixing to recording was 30−40 s. Radical production and decomposition was followed in a mixture containing 500 nM rCiP, 0.5 mM H_2O_2 and 0.2 mM **1a** in three buffer solutions: 50 mM acetate pH = 5.5, 50 mM phosphate pH = 7.0, and 50 mM borate pH = 8.5. The signal amplitude was monitored in the static field of 3460.78 G and with the parameters: frequency 9.7459 GHz, modulation frequency 100 kHz, modulation amplitude 2.5 G, power 0.6362 mW, receiver gain 1.12e5, time constant 1.31072.

Ab initio Calculations of electronic structures and the energies of the AHAs were performed using a Gaussian 94 W package.[32] Geometry optimization of the substrates was accomplished using HF (Hartree−Fock) theory and a 3-21G basis set. The optimized geometry of molecules was used for energies and charges calculations with a 6-31G basis set using RHF and B3PW91 (Density Functional Theory). The atom charges of molecules were calculated using a Mulliken algorithm. The geometry the radicals were calculated with ROHF and a 3-21G basis set. Bond orders were calculated according Pauling bond order expression [Equation (10)] where n is bond order, R(1) and R(n) are bond lengths (in Å) for bonds of unit bond order and n, respectively. The simulations of substrate docking in the active center of *Arthromyces ramosus* peroxidase (ARP) were performed with AutoDock 3.0.[33−35] The crystal data of the ARP (1ARP) and ARP/BHA (1HSR) complexes[19,36] were downloaded from the Protein Data Bank. All water molecules in the active center of ARP were removed with exception of a water molecule on the distal side of the heme. Atomic-interaction energy grid maps were calculated with 0.25 Å grid spacing and 100 grid points forming 25 Å cubic box centered on the active site of peroxidases on heme side exposed to water. The space of the cubic box covered the active site of peroxidases and the space beyond. The electrostatic interaction energy grid used a distance-dependent dielectric function of Mehler−Solmajer.[37] The docking was accomplished using a genetic Lamarckian algorithm. The number of individuals in populations was set to 50. The maximum number of energy evaluations that the genetic algorithm could make was 250 000. The maximum number of generations was 27000. The number of the top individuals that are guaranteed to survive into the next generation was 1. Crossover rate and mutation rate was 0.02 and 0.80, respectively.

$$n = \exp\left(\frac{R(1) - R(n)}{0.3}\right) \quad (10)$$

Acknowledgments

The authors express their sincere thanks to MEMPHYS − Membrane and Statistical Physics Group, Department of Chemistry, the Technical University of Denmark, for kindly letting us use their ESR instrument. We also wish to thank Rie Kristine Schjeltved and Christine Ludvigsen for technical assistance and Arthur J. Olson for supplying AutoDock 3.0 for the substrates docking calculations.

[1] J. Everse, K. E. Everse (Eds.), *Peroxidases in Chemistry and Biology*, CRC Press, Boca Raton, **1991**, vol. 2, pp. 1−25..
[2] T. Ruzgas, E. Csoregi, J. Emneus, L. Gorton, G. Marko-Varga, *Anal. Chim. Acta* **1996**, *330*, 123−138.
[3] H. P. Call, I. Mücke, *J. Biotechnol.* **1997**, *53*, 163−202.
[4] M. Chivukula, V. Renganathan, *Appl. Environ. Microbiol.* **1995**, *61*, 4374−4377.
[5] M. B. Andersen, Y. Hsuanyu, K. G. Welinder, P. Schneider, H. B. Dunford, *Acta Chim. Scand.* **1991**, *45*, 1080−1086.
[6] J. R. Cherry, M. H. Lamsa, P. Schneider, J. Vind, A. Svendsen, A. Jones, A. H. Pedersen, *Nature Biotechnol.* **1999**, *17*, 379−384.
[7] H. B. Dunford, A. J. Adeniran, *Arch. Biochem. Biophys.* **1986**, *251*, 536−542.
[8] M. F. Hughes, B. J. Smith, T. E. Eling, *Chem. Res. Toxicol.* **1992**, *5*, 340−345.
[9] K. Krikstopaitis, J. Kulys, A. H. Pedersen, P. Schneider, *Acta Chem. Scand.* **1998**, *52*, 469−474.
[10] P. P. Kelder, N. J. de Mol, M. J. E. Fischer, L. H. M. Janssen, *Biochim. Biophys. Acta* **1994**, *1205*, 230−238.
[11] J. Kulys, K. Krikstopaitis, A. Ziemys, *J. Biol. Inorg. Chem.* **2000**, *5*, 333−340.
[12] K. Krikstopaitis, J. Kulys, A. Palaima, *Biologija* **1996**, *4*, 33−38.
[13] P. Schneider, H.-J. Deussen, *Int. Patent application* WO99/57360.
[14] A. Carrington, A. D. McLachlan, *Introduction to Magnetic Resonance with Applications to Chemistry and Chemical Physics*, Harper & Row Publishers, New York, Evanston and London, **1967**.
[15] K. Tsukamoto, H. Itakura, K. Sato, K. Fukuyama, S. Miura, S. Takahashi, H. Ikezawa, T. Hosoya, *Biochemistry* **1999**, *38*, 12558−12568.
[16] L. P. Candeias, L. K. Folkes, M. Porssa, J. Parrick, P. Wardman, *Biochemistry* **1996**, *35*, 102−108.
[17] R. A. Marcus, N. Sutin, *Biochim. Biophys. Acta* **1985**, *811*, 265−322.
[18] J.F.W. Petersen, A. Kadziola, S. Larsen, *FEBS Lett.* **1994**, *339*, 291−296.
[19] H. Itakura, Y. Oda, K. Fukuyama, *FEBS Lett.* **1997**, *412*, 107−110.
[20] P. W. Oxley, B. M. Adger, M. J. Sasse, M. A. Forth, *Org. Synth.* **1989**, *67*, 187−192.

[21] S. A. Matlin, P. G. Sammes, R. M. Upton, *J. Chem. Soc., Perkin Trans.* **1979**, *1*, 2481−2487.
[22] C. Poth Brink, A.C. Crumbliss, *J. Org. Chem.* **1982**, *47*, 1171−1176.
[23] K. Healey, C. Calder, *Aust. J. Chem.* **1979**, *32*, 1307−1316.
[24] M. B. Gemborys, G. W. Gribble, *J. Med. Chem.* **1978**, *21*, 649−652.
[25] L. Horner, H. Steppan, *Justus Liebigs Ann. Chem.* **1957**, *606*, 24−47.
[26] J.P.C. Jaimini, N.C. Sogani, *J. Indian Chem. Soc.* **1970**, *47*, 247−250.
[27] O. Neunhoeffner, R. Gottschlich, *Justus Liebigs Ann. Chem.* **1970**, *736*, 100−109.
[28] G. D. Lutwick, D. E. Ryan, *Can. J. Chem.* **1954**, *32*, 949−955.
[29] T. Sakurai, H. Yamamoto, S. Yamada, H. Inoue, *Bull. Chem. Soc. Jpn.* **1985**, *58*, 1174−1181.
[30] K. N. Munshi, V. W. Kharche, H. D. Juneja, *Indian J. Chem. Sect. A* **1988**, *27*, 222−224.
[31] D. Nelson, L. A. Kiesow, *Anal. Biochem.* **1972**, *49*, 474−478.
[32] M. J. Frisch, G. W. Trucks, H. B. Schlegel, P. M. W. Gill, B. G., Johnson, M. A. Robb, J. R. Cheeseman, T. Keith, G. A. Petersson, J. A. Montgomery, K. Raghavachari, M. A. Al-Laham, V. G. Zakrzewski, J. V. Ortiz, J. B. Foresman, J. Cioslowski, B. B. Stefanov, A. Nanayakkara, M. Challacombe, C. Y. Peng, P. Y. Ayala, W. Chen, M. W. Wong, J. L. Andres, E. S. Replogle, R. Gomperts, R. L. Martin, D. J. Fox, J. S. Binkley, D. J. Defrees, J. Baker, J. P. Stewart, M. Head-Gordon, C. Gonzalez, J. A. Pople, *Gaussian 94, Revision E.1*, Gaussian, Inc., Pittsburgh PA, **1995**.
[33] D. S. Goodsell, A. J. Olson, *Prot. Struct. Func. Gen.* **1990**, *8*, 195−202.
[34] G. M. Morris, D. S. Goodsell, R. Huey, A. J. Olson, *J. Com. Aid. Mol. Des.* **1996**, *10*, 293−304.
[35] G. M. Morris, D. S. Goodsell, R. S. Halliday, R. Huey, W. E. Hart, R. K. Belew, A. J. Olson, *J. Comp. Chem.* **1998**, *19*, 1639−1662.
[36] N. Kunishima, K. Fukuyama, H. Matsubara, H. Hatanaka, Y. Shibano, T. Amachi, *J. Mol. Biol.* **1994**, *235*, 331−344.
[37] E. L. Mehler, T. Solmajer, *Protein. Eng.* **1991**, *4*, 903−910.

Received March 7, 2001
[O01111]